BABAR-CONF-06/035
SLAC-PUB-11980
hep-ex/0607042
July 2006

A Study of $\Xi_c(2980)^+$ and $\Xi_c(3077)^+$

The *BABAR* Collaboration

July 26, 2006

Abstract

We present a study of two states decaying to $\Lambda_c^+ K^- \pi^+$ using the *BABAR* detector at the SLAC PEP-II asymmetric-energy e^+e^- storage rings. We use an integrated luminosity of $288.5\,\mathrm{fb}^{-1}$ collected at the center-of-mass energy $\sqrt{s} = 10.58$ GeV, near the peak of the $\Upsilon(4S)$ resonance, plus $27.2\,\mathrm{fb}^{-1}$ collected approximately 40 MeV below this energy. We search for the particles $\Xi_c(2980)^+$ and $\Xi_c(3077)^+$, recently discovered by the Belle Collaboration, in their decays to $\Lambda_c^+ K^- \pi^+$, where $\Lambda_c^+ \to pK^-\pi^+$. We find a signal with $7.0\,\sigma$ significance for the $\Xi_c(2980)^+$ state with a mass difference with respect to the Λ_c^+ of $(680.6 \pm 1.9 \pm 1.0)\,\mathrm{MeV}/c^2$ (first error is statistical and second error is systematic). The measured width for this state is $(23.6 \pm 2.8 \pm 1.3)$ MeV, and the yield is $284 \pm 45 \pm 46$ events. We find a signal with $8.6\,\sigma$ significance for the $\Xi_c(3077)^+$ state with a mass difference with respect to the Λ_c^+ of $(790.0 \pm 0.7 \pm 0.2)\,\mathrm{MeV}/c^2$, a width of $(6.2 \pm 1.6 \pm 0.5)$ MeV, and a yield of $204 \pm 35 \pm 12$ events. The $\Xi_c(2980)^+$ is found to decay resonantly through the intermediate state $\Sigma_c(2455)^{++}K^-$ with $4.9\,\sigma$ significance and non-resonantly to $\Lambda_c^+ K^- \pi^+$ with $4.1\,\sigma$ significance. With $5.8\,\sigma$ significance, the $\Xi_c(3077)^+$ is found to decay resonantly through $\Sigma_c(2455)^{++}K^-$, and with $4.6\,\sigma$ significance, it is found to decay through $\Sigma_c(2520)^{++}K^-$. The significance of the signal for the non-resonant decay $\Xi_c(3077)^+ \to \Lambda_c^+ K^- \pi^+$ is $1.4\,\sigma$. These results are preliminary.

Submitted to the 33$^{\mathrm{nd}}$ International Conference on High-Energy Physics, ICHEP 06,
26 July—2 August 2006, Moscow, Russia.

Stanford Linear Accelerator Center, Stanford University, Stanford, CA 94309

Work supported in part by Department of Energy contract DE-AC02-76SF00515

The *BABAR* Collaboration,

B. Aubert, R. Barate, M. Bona, D. Boutigny, F. Couderc, Y. Karyotakis, J. P. Lees, V. Poireau, V. Tisserand, A. Zghiche

Laboratoire de Physique des Particules, IN2P3/CNRS et Université de Savoie, F-74941 Annecy-Le-Vieux, France

E. Grauges

Universitat de Barcelona, Facultat de Fisica, Departament ECM, E-08028 Barcelona, Spain

A. Palano

Università di Bari, Dipartimento di Fisica and INFN, I-70126 Bari, Italy

J. C. Chen, N. D. Qi, G. Rong, P. Wang, Y. S. Zhu

Institute of High Energy Physics, Beijing 100039, China

G. Eigen, I. Ofte, B. Stugu

University of Bergen, Institute of Physics, N-5007 Bergen, Norway

G. S. Abrams, M. Battaglia, D. N. Brown, J. Button-Shafer, R. N. Cahn, E. Charles, M. S. Gill, Y. Groysman, R. G. Jacobsen, J. A. Kadyk, L. T. Kerth, Yu. G. Kolomensky, G. Kukartsev, G. Lynch, L. M. Mir, T. J. Orimoto, M. Pripstein, N. A. Roe, M. T. Ronan, W. A. Wenzel

Lawrence Berkeley National Laboratory and University of California, Berkeley, California 94720, USA

P. del Amo Sanchez, M. Barrett, K. E. Ford, A. J. Hart, T. J. Harrison, C. M. Hawkes, S. E. Morgan, A. T. Watson

University of Birmingham, Birmingham, B15 2TT, United Kingdom

T. Held, H. Koch, B. Lewandowski, M. Pelizaeus, K. Peters, T. Schroeder, M. Steinke

Ruhr Universität Bochum, Institut für Experimentalphysik 1, D-44780 Bochum, Germany

J. T. Boyd, J. P. Burke, W. N. Cottingham, D. Walker

University of Bristol, Bristol BS8 1TL, United Kingdom

D. J. Asgeirsson, T. Cuhadar-Donszelmann, B. G. Fulsom, C. Hearty, N. S. Knecht, T. S. Mattison, J. A. McKenna

University of British Columbia, Vancouver, British Columbia, Canada V6T 1Z1

A. Khan, P. Kyberd, M. Saleem, D. J. Sherwood, L. Teodorescu

Brunel University, Uxbridge, Middlesex UB8 3PH, United Kingdom

V. E. Blinov, A. D. Bukin, V. P. Druzhinin, V. B. Golubev, A. P. Onuchin, S. I. Serednyakov, Yu. I. Skovpen, E. P. Solodov, K. Yu Todyshev

Budker Institute of Nuclear Physics, Novosibirsk 630090, Russia

D. S. Best, M. Bondioli, M. Bruinsma, M. Chao, S. Curry, I. Eschrich, D. Kirkby, A. J. Lankford, P. Lund, M. Mandelkern, R. K. Mommsen, W. Roethel, D. P. Stoker

University of California at Irvine, Irvine, California 92697, USA

S. Abachi, C. Buchanan

University of California at Los Angeles, Los Angeles, California 90024, USA

S. D. Foulkes, J. W. Gary, O. Long, B. C. Shen, K. Wang, L. Zhang
University of California at Riverside, Riverside, California 92521, USA

H. K. Hadavand, E. J. Hill, H. P. Paar, S. Rahatlou, V. Sharma
University of California at San Diego, La Jolla, California 92093, USA

J. W. Berryhill, C. Campagnari, A. Cunha, B. Dahmes, T. M. Hong, D. Kovalskyi, J. D. Richman
University of California at Santa Barbara, Santa Barbara, California 93106, USA

T. W. Beck, A. M. Eisner, C. J. Flacco, C. A. Heusch, J. Kroseberg, W. S. Lockman, G. Nesom, T. Schalk, B. A. Schumm, A. Seiden, P. Spradlin, D. C. Williams, M. G. Wilson
University of California at Santa Cruz, Institute for Particle Physics, Santa Cruz, California 95064, USA

J. Albert, E. Chen, A. Dvoretskii, F. Fang, D. G. Hitlin, I. Narsky, T. Piatenko, F. C. Porter, A. Ryd, A. Samuel
California Institute of Technology, Pasadena, California 91125, USA

G. Mancinelli, B. T. Meadows, K. Mishra, M. D. Sokoloff
University of Cincinnati, Cincinnati, Ohio 45221, USA

F. Blanc, P. C. Bloom, S. Chen, W. T. Ford, J. F. Hirschauer, A. Kreisel, M. Nagel, U. Nauenberg, A. Olivas, W. O. Ruddick, J. G. Smith, K. A. Ulmer, S. R. Wagner, J. Zhang
University of Colorado, Boulder, Colorado 80309, USA

A. Chen, E. A. Eckhart, A. Soffer, W. H. Toki, R. J. Wilson, F. Winklmeier, Q. Zeng
Colorado State University, Fort Collins, Colorado 80523, USA

D. D. Altenburg, E. Feltresi, A. Hauke, H. Jasper, J. Merkel, A. Petzold, B. Spaan
Universität Dortmund, Institut für Physik, D-44221 Dortmund, Germany

T. Brandt, V. Klose, H. M. Lacker, W. F. Mader, R. Nogowski, J. Schubert, K. R. Schubert, R. Schwierz, J. E. Sundermann, A. Volk
Technische Universität Dresden, Institut für Kern- und Teilchenphysik, D-01062 Dresden, Germany

D. Bernard, G. R. Bonneaud, E. Latour, Ch. Thiebaux, M. Verderi
Laboratoire Leprince-Ringuet, CNRS/IN2P3, Ecole Polytechnique, F-91128 Palaiseau, France

P. J. Clark, W. Gradl, F. Muheim, S. Playfer, A. I. Robertson, Y. Xie
University of Edinburgh, Edinburgh EH9 3JZ, United Kingdom

M. Andreotti, D. Bettoni, C. Bozzi, R. Calabrese, G. Cibinetto, E. Luppi, M. Negrini, A. Petrella, L. Piemontese, E. Prencipe
Università di Ferrara, Dipartimento di Fisica and INFN, I-44100 Ferrara, Italy

F. Anulli, R. Baldini-Ferroli, A. Calcaterra, R. de Sangro, G. Finocchiaro, S. Pacetti, P. Patteri, I. M. Peruzzi,[1] M. Piccolo, M. Rama, A. Zallo
Laboratori Nazionali di Frascati dell'INFN, I-00044 Frascati, Italy

[1]Also with Università di Perugia, Dipartimento di Fisica, Perugia, Italy

A. Buzzo, R. Capra, R. Contri, M. Lo Vetere, M. M. Macri, M. R. Monge, S. Passaggio, C. Patrignani, E. Robutti, A. Santroni, S. Tosi

Università di Genova, Dipartimento di Fisica and INFN, I-16146 Genova, Italy

G. Brandenburg, K. S. Chaisanguanthum, M. Morii, J. Wu

Harvard University, Cambridge, Massachusetts 02138, USA

R. S. Dubitzky, J. Marks, S. Schenk, U. Uwer

Universität Heidelberg, Physikalisches Institut, Philosophenweg 12, D-69120 Heidelberg, Germany

D. J. Bard, W. Bhimji, D. A. Bowerman, P. D. Dauncey, U. Egede, R. L. Flack, J. A. Nash, M. B. Nikolich, W. Panduro Vazquez

Imperial College London, London, SW7 2AZ, United Kingdom

P. K. Behera, X. Chai, M. J. Charles, U. Mallik, N. T. Meyer, V. Ziegler

University of Iowa, Iowa City, Iowa 52242, USA

J. Cochran, H. B. Crawley, L. Dong, V. Eyges, W. T. Meyer, S. Prell, E. I. Rosenberg, A. E. Rubin

Iowa State University, Ames, Iowa 50011-3160, USA

A. V. Gritsan

Johns Hopkins University, Baltimore, Maryland 21218, USA

A. G. Denig, M. Fritsch, G. Schott

Universität Karlsruhe, Institut für Experimentelle Kernphysik, D-76021 Karlsruhe, Germany

N. Arnaud, M. Davier, G. Grosdidier, A. Höcker, F. Le Diberder, V. Lepeltier, A. M. Lutz, A. Oyanguren, S. Pruvot, S. Rodier, P. Roudeau, M. H. Schune, A. Stocchi, W. F. Wang, G. Wormser

Laboratoire de l'Accélérateur Linéaire, IN2P3/CNRS et Université Paris-Sud 11, Centre Scientifique d'Orsay, B.P. 34, F-91898 ORSAY Cedex, France

C. H. Cheng, D. J. Lange, D. M. Wright

Lawrence Livermore National Laboratory, Livermore, California 94550, USA

C. A. Chavez, I. J. Forster, J. R. Fry, E. Gabathuler, R. Gamet, K. A. George, D. E. Hutchcroft, D. J. Payne, K. C. Schofield, C. Touramanis

University of Liverpool, Liverpool L69 7ZE, United Kingdom

A. J. Bevan, F. Di Lodovico, W. Menges, R. Sacco

Queen Mary, University of London, E1 4NS, United Kingdom

G. Cowan, H. U. Flaecher, D. A. Hopkins, P. S. Jackson, T. R. McMahon, S. Ricciardi, F. Salvatore, A. C. Wren

University of London, Royal Holloway and Bedford New College, Egham, Surrey TW20 0EX, United Kingdom

D. N. Brown, C. L. Davis

University of Louisville, Louisville, Kentucky 40292, USA

J. Allison, N. R. Barlow, R. J. Barlow, Y. M. Chia, C. L. Edgar, G. D. Lafferty, M. T. Naisbit, J. C. Williams, J. I. Yi

University of Manchester, Manchester M13 9PL, United Kingdom

C. Chen, W. D. Hulsbergen, A. Jawahery, C. K. Lae, D. A. Roberts, G. Simi

University of Maryland, College Park, Maryland 20742, USA

G. Blaylock, C. Dallapiccola, S. S. Hertzbach, X. Li, T. B. Moore, S. Saremi, H. Staengle

University of Massachusetts, Amherst, Massachusetts 01003, USA

R. Cowan, G. Sciolla, S. J. Sekula, M. Spitznagel, F. Taylor, R. K. Yamamoto

Massachusetts Institute of Technology, Laboratory for Nuclear Science, Cambridge, Massachusetts 02139, USA

H. Kim, S. E. Mclachlin, P. M. Patel, S. H. Robertson

McGill University, Montréal, Québec, Canada H3A 2T8

A. Lazzaro, V. Lombardo, F. Palombo

Università di Milano, Dipartimento di Fisica and INFN, I-20133 Milano, Italy

J. M. Bauer, L. Cremaldi, V. Eschenburg, R. Godang, R. Kroeger, D. A. Sanders, D. J. Summers, H. W. Zhao

University of Mississippi, University, Mississippi 38677, USA

S. Brunet, D. Côté, M. Simard, P. Taras, F. B. Viaud

Université de Montréal, Physique des Particules, Montréal, Québec, Canada H3C 3J7

H. Nicholson

Mount Holyoke College, South Hadley, Massachusetts 01075, USA

N. Cavallo,[2] G. De Nardo, F. Fabozzi,[3] C. Gatto, L. Lista, D. Monorchio, P. Paolucci, D. Piccolo, C. Sciacca

Università di Napoli Federico II, Dipartimento di Scienze Fisiche and INFN, I-80126, Napoli, Italy

M. A. Baak, G. Raven, H. L. Snoek

NIKHEF, National Institute for Nuclear Physics and High Energy Physics, NL-1009 DB Amsterdam, The Netherlands

C. P. Jessop, J. M. LoSecco

University of Notre Dame, Notre Dame, Indiana 46556, USA

T. Allmendinger, G. Benelli, L. A. Corwin, K. K. Gan, K. Honscheid, D. Hufnagel, P. D. Jackson, H. Kagan, R. Kass, A. M. Rahimi, J. J. Regensburger, R. Ter-Antonyan, Q. K. Wong

Ohio State University, Columbus, Ohio 43210, USA

N. L. Blount, J. Brau, R. Frey, O. Igonkina, J. A. Kolb, M. Lu, R. Rahmat, N. B. Sinev, D. Strom, J. Strube, E. Torrence

University of Oregon, Eugene, Oregon 97403, USA

[2]Also with Università della Basilicata, Potenza, Italy
[3]Also with Università della Basilicata, Potenza, Italy

A. Gaz, M. Margoni, M. Morandin, A. Pompili, M. Posocco, M. Rotondo, F. Simonetto, R. Stroili, C. Voci
Università di Padova, Dipartimento di Fisica and INFN, I-35131 Padova, Italy

M. Benayoun, H. Briand, J. Chauveau, P. David, L. Del Buono, Ch. de la Vaissière, O. Hamon, B. L. Hartfiel, M. J. J. John, Ph. Leruste, J. Malclès, J. Ocariz, L. Roos, G. Therin
Laboratoire de Physique Nucléaire et de Hautes Energies, IN2P3/CNRS, Université Pierre et Marie Curie-Paris6, Université Denis Diderot-Paris7, F-75252 Paris, France

L. Gladney, J. Panetta
University of Pennsylvania, Philadelphia, Pennsylvania 19104, USA

M. Biasini, R. Covarelli
Università di Perugia, Dipartimento di Fisica and INFN, I-06100 Perugia, Italy

C. Angelini, G. Batignani, S. Bettarini, F. Bucci, G. Calderini, M. Carpinelli, R. Cenci, F. Forti, M. A. Giorgi, A. Lusiani, G. Marchiori, M. A. Mazur, M. Morganti, N. Neri, E. Paoloni, G. Rizzo, J. J. Walsh
Università di Pisa, Dipartimento di Fisica, Scuola Normale Superiore and INFN, I-56127 Pisa, Italy

M. Haire, D. Judd, D. E. Wagoner
Prairie View A&M University, Prairie View, Texas 77446, USA

J. Biesiada, N. Danielson, P. Elmer, Y. P. Lau, C. Lu, J. Olsen, A. J. S. Smith, A. V. Telnov
Princeton University, Princeton, New Jersey 08544, USA

F. Bellini, G. Cavoto, A. D'Orazio, D. del Re, E. Di Marco, R. Faccini, F. Ferrarotto, F. Ferroni, M. Gaspero, L. Li Gioi, M. A. Mazzoni, S. Morganti, G. Piredda, F. Polci, F. Safai Tehrani, C. Voena
Università di Roma La Sapienza, Dipartimento di Fisica and INFN, I-00185 Roma, Italy

M. Ebert, H. Schröder, R. Waldi
Universität Rostock, D-18051 Rostock, Germany

T. Adye, N. De Groot, B. Franek, E. O. Olaiya, F. F. Wilson
Rutherford Appleton Laboratory, Chilton, Didcot, Oxon, OX11 0QX, United Kingdom

R. Aleksan, S. Emery, A. Gaidot, S. F. Ganzhur, G. Hamel de Monchenault, W. Kozanecki, M. Legendre, G. Vasseur, Ch. Yèche, M. Zito
DSM/Dapnia, CEA/Saclay, F-91191 Gif-sur-Yvette, France

X. R. Chen, H. Liu, W. Park, M. V. Purohit, J. R. Wilson
University of South Carolina, Columbia, South Carolina 29208, USA

M. T. Allen, D. Aston, R. Bartoldus, P. Bechtle, N. Berger, R. Claus, J. P. Coleman, M. R. Convery, M. Cristinziani, J. C. Dingfelder, J. Dorfan, G. P. Dubois-Felsmann, D. Dujmic, W. Dunwoodie, R. C. Field, T. Glanzman, S. J. Gowdy, M. T. Graham, P. Grenier,[4] V. Halyo, C. Hast, T. Hryn'ova, W. R. Innes, M. H. Kelsey, P. Kim, D. W. G. S. Leith, S. Li, S. Luitz, V. Luth, H. L. Lynch, D. B. MacFarlane, H. Marsiske, R. Messner, D. R. Muller, C. P. O'Grady, V. E. Ozcan, A. Perazzo, M. Perl, T. Pulliam, B. N. Ratcliff, A. Roodman, A. A. Salnikov, R. H. Schindler, J. Schwiening, A. Snyder, J. Stelzer, D. Su, M. K. Sullivan, K. Suzuki, S. K. Swain, J. M. Thompson, J. Va'vra, N. van

[4]Also at Laboratoire de Physique Corpusculaire, Clermont-Ferrand, France

Bakel, M. Weaver, A. J. R. Weinstein, W. J. Wisniewski, M. Wittgen, D. H. Wright, A. K. Yarritu, K. Yi, C. C. Young
Stanford Linear Accelerator Center, Stanford, California 94309, USA

P. R. Burchat, A. J. Edwards, S. A. Majewski, B. A. Petersen, C. Roat, L. Wilden
Stanford University, Stanford, California 94305-4060, USA

S. Ahmed, M. S. Alam, R. Bula, J. A. Ernst, V. Jain, B. Pan, M. A. Saeed, F. R. Wappler, S. B. Zain
State University of New York, Albany, New York 12222, USA

W. Bugg, M. Krishnamurthy, S. M. Spanier
University of Tennessee, Knoxville, Tennessee 37996, USA

R. Eckmann, J. L. Ritchie, A. Satpathy, C. J. Schilling, R. F. Schwitters
University of Texas at Austin, Austin, Texas 78712, USA

J. M. Izen, X. C. Lou, S. Ye
University of Texas at Dallas, Richardson, Texas 75083, USA

F. Bianchi, F. Gallo, D. Gamba
Università di Torino, Dipartimento di Fisica Sperimentale and INFN, I-10125 Torino, Italy

M. Bomben, L. Bosisio, C. Cartaro, F. Cossutti, G. Della Ricca, S. Dittongo, L. Lanceri, L. Vitale
Università di Trieste, Dipartimento di Fisica and INFN, I-34127 Trieste, Italy

V. Azzolini, N. Lopez-March, F. Martinez-Vidal
IFIC, Universitat de Valencia-CSIC, E-46071 Valencia, Spain

Sw. Banerjee, B. Bhuyan, C. M. Brown, D. Fortin, K. Hamano, R. Kowalewski, I. M. Nugent, J. M. Roney, R. J. Sobie
University of Victoria, Victoria, British Columbia, Canada V8W 3P6

J. J. Back, P. F. Harrison, T. E. Latham, G. B. Mohanty, M. Pappagallo
Department of Physics, University of Warwick, Coventry CV4 7AL, United Kingdom

H. R. Band, X. Chen, B. Cheng, S. Dasu, M. Datta, K. T. Flood, J. J. Hollar, P. E. Kutter, B. Mellado, A. Mihalyi, Y. Pan, M. Pierini, R. Prepost, S. L. Wu, Z. Yu
University of Wisconsin, Madison, Wisconsin 53706, USA

H. Neal
Yale University, New Haven, Connecticut 06511, USA

1 INTRODUCTION

The Belle Collaboration has recently reported evidence for two new charm baryon states [1, 2]. These two new states have been called the $\Xi_c(2980)^+$ and the $\Xi_c(3077)^+$. Belle finds evidence for these states at $(2978.5 \pm 2.1 \pm 2.0)\,\mathrm{MeV}/c^2$ and $(3076.7 \pm 0.9 \pm 0.5)\,\mathrm{MeV}/c^2$ in the $\Lambda_c^+ K^- \pi^+$ invariant mass spectrum and quotes statistical significances greater than $6\,\sigma$ for both states. They also find significant signal for the isospin partner $\Xi_c(3077)^0$ in the $\Lambda_c^+ K_S^0 \pi^-$ invariant mass spectrum.

Previously known excited Ξ_c baryons have only been observed in decays to lower-mass Ξ_c baryons plus a pion or gamma. These two new states decay such that the charm and strange quarks are contained in separate hadrons. This type of decay may have implications for the internal quark dynamics of these two new states.

In the analysis described here, we find yields for $\Xi_c(2980)^+$ and $\Xi_c(3077)^+$ in their decays to $\Lambda_c^+ K^- \pi^+$, where $\Lambda_c^+ \to p K^- \pi^+$. The mass differences with respect to the Λ_c^+ baryon and the widths of $\Xi_c(2980)^+$ and $\Xi_c(3077)^+$ are also measured. The Dalitz-plot structure of the $\Xi_c(2980)^+$ and the $\Xi_c(3077)^+$ three-body decays are also studied. The statistical significance of resonant decays through $\Sigma_c(2455)^{++} K^-$ and $\Sigma_c(2520)^{++} K^-$ are calculated, and the signal yields for both resonant and non-resonant decays are measured.

2 THE *BaBar* DETECTOR AND DATASET

We use $288.5\,\mathrm{fb}^{-1}$ of data collected at $\sqrt{s} = 10.58$ GeV plus $27.2\,\mathrm{fb}^{-1}$ of data collected approximately 40 MeV below this energy. The *BABAR* detector, located at the SLAC PEP-II asymmetric-energy e^+e^- storage rings, was used to collect this data. The *BABAR* detector is described in detail elsewhere [3]. The tracking of charged particles is provided by a five-layer double-sided silicon vertex tracker (SVT) and a 40-layer drift chamber (DCH). Discrimination among charged pions, kaons, and protons relies on ionization energy loss ($\mathrm{d}E/\mathrm{d}x$) in the DCH and SVT, and on Cherenkov photons detected in a ring-imaging detector (DIRC). A CsI(Tl) crystal calorimeter is used to identify electrons and photons. These four detector subsystems are mounted inside a 1.5-T solenoidal superconducting magnet. The instrumented flux return for the solenoidal magnet provides muon identification.

For signal event simulations, we use the Monte Carlo (MC) generators JETSET74 [4] and EVTGEN [5] with a full detector simulation based on GEANT4 [6]. These simulations are used to estimate the reconstruction efficiencies and detector resolutions. The efficiencies in our analysis for finding simulated $\Xi_c(2980)^+$ and $\Xi_c(3077)^+$ decays to $\Lambda_c^+ K^- \pi^+$, where $\Lambda_c^+ \to p K^- \pi^+$, are roughly 10%.

3 ANALYSIS METHOD

Λ_c^+ candidates are formed from the geometrical combination of p, K^-, and π^+ tracks. $\Xi_c(2980)^+$ and $\Xi_c(3077)^+$ candidates are formed from combining the Λ_c^+ candidates with additional K^- and π^+ tracks. The $pK^-\pi^+$ and $\Lambda_c^+ K^- \pi^+$ vertices are fit simultaneously. The selection criteria, based on particle identification likelihood ratios, track qualities (tracks within 1.5 cm of the beam spot and with DCH information), and the χ^2 probability for fitted vertices ($P(\chi^2) > 1\%$), are designed to maximize $\epsilon/\sqrt{B}$. The value of ϵ is the simulated signal reconstruction efficiency and B is the number of background candidates in data. The Λ_c^+ candidate mass is required to be within $10\,\mathrm{MeV}/c^2$ (2.1σ) of $2286\,\mathrm{MeV}/c^2$ (the fitted mean of the Λ_c^+ signal in the data) as illustrated in

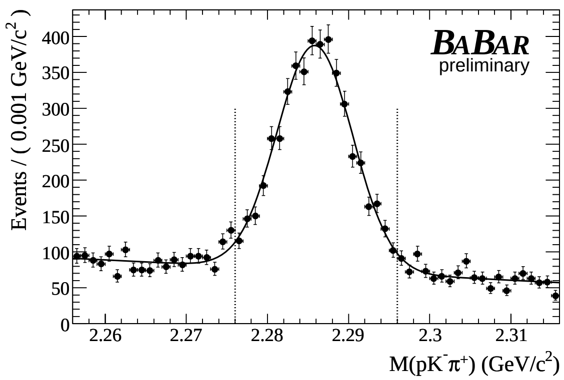

Figure 1: The $pK^-\pi^+$ invariant mass distribution for signal candidates in data. The curve depicts an unbinned likelihood fit to a Gaussian plus a line. The dotted vertical lines are $\pm 10\,\mathrm{MeV}/c^2$ ($\pm 2.1\ \sigma$) from the mean of the fitted Gaussian ($2286\,\mathrm{MeV}/c^2$).

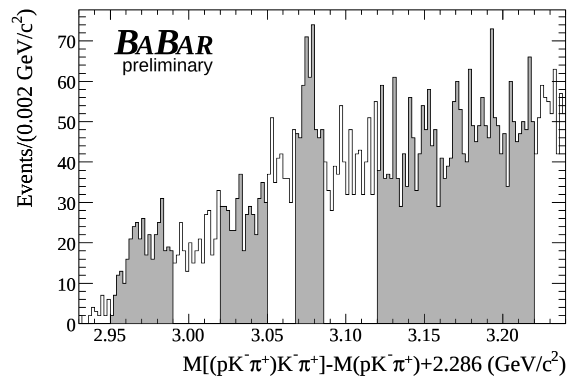

Figure 2: The distribution of the invariant mass difference M_{Ξ_c} for signal candidates in data. The shaded regions are used for the Dalitz plots illustrated in Figure 3.

Figure 1. Charm hadrons carry a significant fraction of the initial energy of the charm quark, whereas random combinations of charged particles in an event form lower-energy candidates. To take advantage of this difference, we select signal candidates that have momentum in the e^+e^- center-of-mass frame greater than $3.0\,\mathrm{GeV}/c$.

Any resonant substructure in a three-body decay mode will alter the signal line shape from that of a decay mode with a uniform phase-space substructure. This is particularly important when the decay in question is near its kinematic threshold. The resonant substructure of the $\Lambda_c^+K^-\pi^+$ combination is studied with Dalitz plots for four ranges of the invariant mass difference

$$M_{\Xi_c} = M[(pK^-\pi^+)K^-\pi^+] - M(pK^-\pi^+) + 2.286\,\mathrm{GeV}/c^2\,. \tag{1}$$

These ranges are illustrated in Figure 2. Candidates around the $\Xi_c(2980)^+$ and $\Xi_c(3077)^+$ signals are selected with the ranges $2.95\,\mathrm{GeV}/c^2 < M_{\Xi_c} < 2.99\,\mathrm{GeV}/c^2$ and $3.07\,\mathrm{GeV}/c^2 < M_{\Xi_c} < 3.09\,\mathrm{GeV}/c^2$, respectively. The ranges $3.02\,\mathrm{GeV}/c^2 < M_{\Xi_c} < 3.05\,\mathrm{GeV}/c^2$ and $3.12\,\mathrm{GeV}/c^2 < M_{\Xi_c} < 3.22\,\mathrm{GeV}/c^2$ are used to select background candidates.

Dalitz plots of $M(\pi^+K^-)^2$ versus $M(\Lambda_c^+\pi^+)^2$ are shown in Figure 3 for each of the M_{Ξ_c} ranges shown in Figure 2. In each of the four sub-figures, $\Lambda_c^+\pi^+$ resonances are visible as vertical bands at $M(\Lambda_c^+\pi^+)^2 \sim 6.02\,\mathrm{GeV}^2/\mathrm{c}^4$ and/or $M(\Lambda_c^+\pi^+)^2 \sim 6.35\,\mathrm{GeV}^2/\mathrm{c}^4$, corresponding to the $\Sigma_c(2455)^{++}$ and $\Sigma_c(2520)^{++}$, respectively. No other significant structures are observed in the Dalitz plots. The presence of the $\Sigma_c(2455)^{++}$ and/or $\Sigma_c(2520)^{++}$ resonances in all four M_{Ξ_c} regions motivates a two-dimensional fit that can account for the effects of these intermediate resonances.

The data is fit in two dimensions of invariant mass difference: M_{Ξ_c}, as defined by Equation 1, and

$$M_{\Sigma_c} = M[(pK^-\pi^+)\pi^+] - M(pK^-\pi^+) + 2.286\,\mathrm{GeV}/c^2\,. \tag{2}$$

An extended unbinned maximum likelihood fit is used in the invariant mass range $2.92\,\mathrm{GeV}/c^2 \lesssim M_{\Xi_c} \lesssim 3.14\,\mathrm{GeV}/c^2$. A scatter plot of the M_{Σ_c} vs. M_{Ξ_c} fit range is shown in Figure 4. The probability density function (PDF) used to fit the data is divided into four types of components.

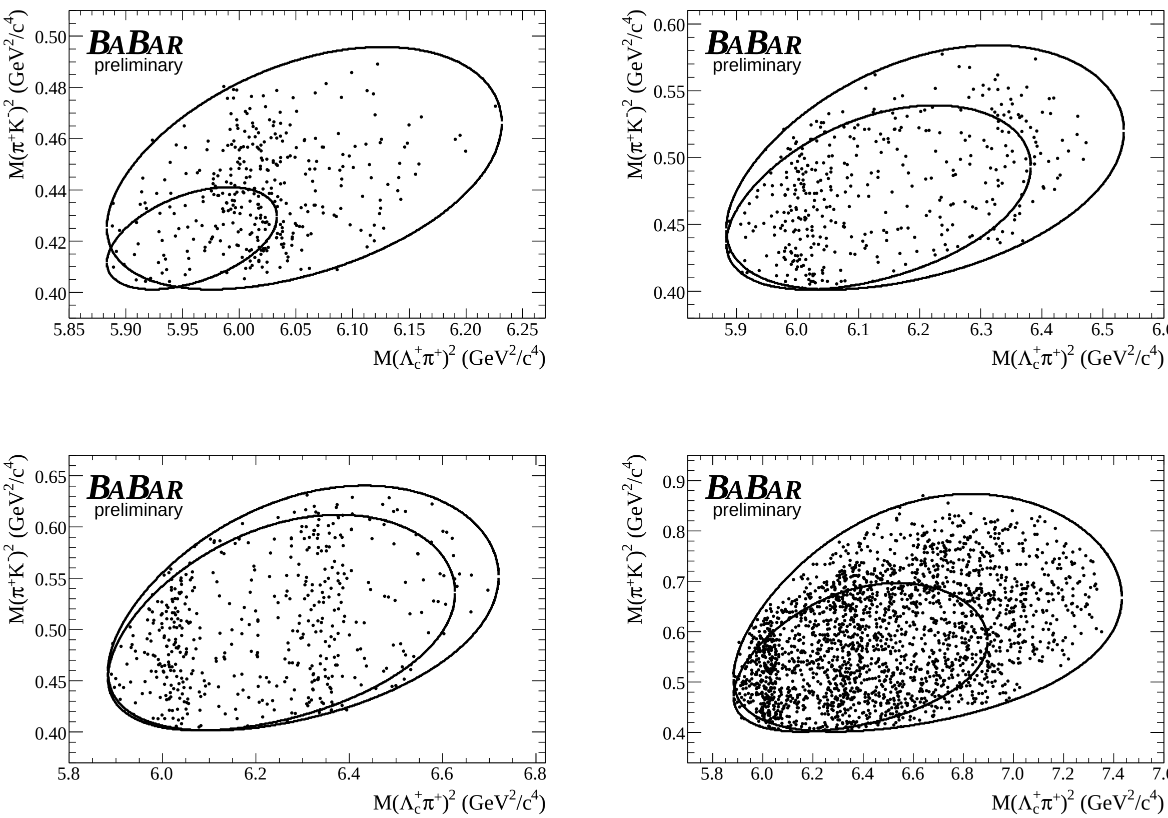

Figure 3: Dalitz plots of $M(\pi^+K^-)^2$ vs. $M(\Lambda_c^+\pi^+)^2$. Data from the four shaded M_{Ξ_c} ranges in Figure 2 are shown in order of increasing mass from left to right, top to bottom. The two curves in each plot represent the kinematic boundaries of the Dalitz plot for M_{Ξ_c} mass values at the lower and upper edges of the M_{Ξ_c} range.

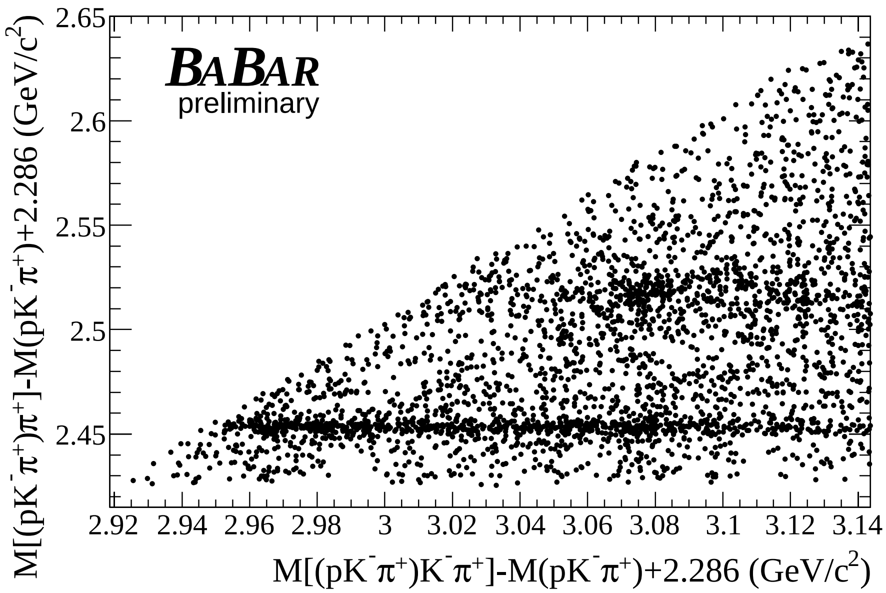

Figure 4: A two-dimensional scatter plot of the M_{Σ_c} vs. M_{Ξ_c} fit range for $pK^-\pi^+K^-\pi^+$ candidates in data. The upper and lower horizontal bands are from the $\Sigma_c(2520)^{++}$ and $\Sigma_c(2455)$ resonances, respectively.

One category is used to fit the non-resonant combinatoric background. Another category is used to fit the combinatoric background with $\Sigma_c(2455)^{++}$ and $\Sigma_c(2520)^{++}$ resonances. The remaining two categories are used to fit the $\Xi_c(2980)^+$ and $\Xi_c(3077)^+$ signals with and without $\Sigma_c(2455)^{++}$ and $\Sigma_c(2520)^{++}$ resonances. Each PDF component is described below.

A $M(pK^-\pi^+)$ sideband sample around the Λ_c^+ mass ($20\,\mathrm{MeV}/c^2 < |M(pK^-\pi^+) - 2286\,\mathrm{MeV}/c^2| < 40\,\mathrm{MeV}/c^2$) and a wrong-sign $\Lambda_c^+K^+\pi^-$ data sample are used to establish the non-resonant and resonant background PDF parameterizations, respectively. Projections of the fit to M_{Ξ_c} and M_{Σ_c} in the $M(pK^-\pi^+)$ sideband sample are shown in Figure 5. The PDF used to fit these sideband data is proportional to a threshold function in M_{Ξ_c} ($T(M_{\Xi_c})$) and the sum of two threshold functions in M_{Σ_c} ($T(M_{\Sigma_c})$):

$$T(M_{\Xi_c}) \times [(1-k)T_a(M_{\Sigma_c}) + kT_b(M_{\Sigma_c})]\,, \tag{3}$$

where k is a free parameter and the subscripts a and b indicate two instances of the same functional form. These threshold functions are of the form

$$T(x) = x\left[-1 + \left(\frac{x}{t}\right)^2\right]^{1/2} \exp\left[-p + p\left(\frac{x}{t}\right)^2\right]\,, \tag{4}$$

where x is the mass variable in which there is a minimum kinematic threshold, t is the mass value of the threshold, and p is a free shape parameter in the fit. For $T(M_{\Sigma_c})$, the threshold t is a constant $2425.6\,\mathrm{MeV}/c^2$. For $T(M_{\Xi_c})$, the threshold is dependent on M_{Σ_c} through the relation $t = M_{\Sigma_c} + m_K$, where m_K is the K^+ mass.

Projections of the fit to M_{Ξ_c} vs. M_{Σ_c} in the wrong-sign data sample are shown in Figure 6. The PDF used to fit this wrong-sign sample has two components. One component is the same

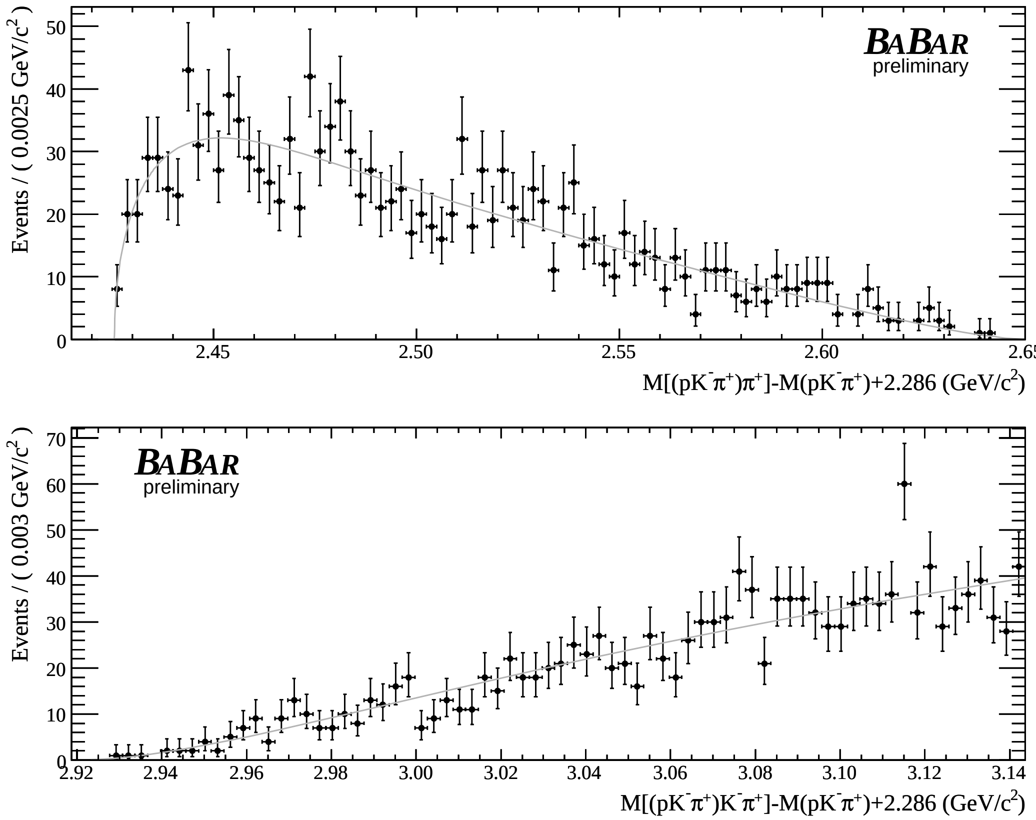

Figure 5: Projections onto the mass variables M_{Σ_c} (upper) and M_{Ξ_c} (lower) for the $M(pK^-\pi^+)$ sideband sample (points with error bars) and a fitted PDF (curves) described in the text (Equation 3).

as the PDF used to fit the sideband data (Equation 3). The other component fits $\Sigma_c(2455)^0$ and $\Sigma_c(2520)^0$ resonances in M_{Σ_c} with non-relativistic Breit-Wigner shapes convolved with Gaussian resolution functions (also known as Voigtian line shapes, $V(M_{\Sigma_c})$), times a two-body phase-space function $F_2(M_{\Sigma_c})$. This second component is proportional to

$$[(1-r)V_a(M_{\Sigma_c}) + rV_b(M_{\Sigma_c})] \times F_2(M_{\Sigma_c}) \times T(M_{\Xi_c})\,, \tag{5}$$

where r is the ratio of the fitted number of candidates in the $\Sigma_c(2520)^0$ resonance to the total fitted number of candidates in both intermediate resonances, the subscripts a and b indicate two instances of the same Voigtian functional form (one for $\Sigma_c(2455)^0$ and one for $\Sigma_c(2520)^0$), and $T(M_{\Xi_c})$ has the same shape parameter as $T(M_{\Xi_c})$ in Equation 3. The two-body phase-space function is

$$F_2(M_{\Sigma_c}) = \frac{[(M_{\Sigma_c}^2 - (m_{\Lambda_c} + m_\pi)^2)(M_{\Sigma_c}^2 - (m_{\Lambda_c} - m_\pi)^2)]^{1/2}}{2M_{\Sigma_c}}\,, \tag{6}$$

where m_{Λ_c} is the Λ_c^+ mass used in Equations 1 and 2 (2286 MeV/c^2), and m_π is the π^+ mass.

For both the wrong-sign sample and the Λ_c^+ sideband sample, the background is described well by the fitted background PDF. The same PDF functional form used for the wrong-sign sample

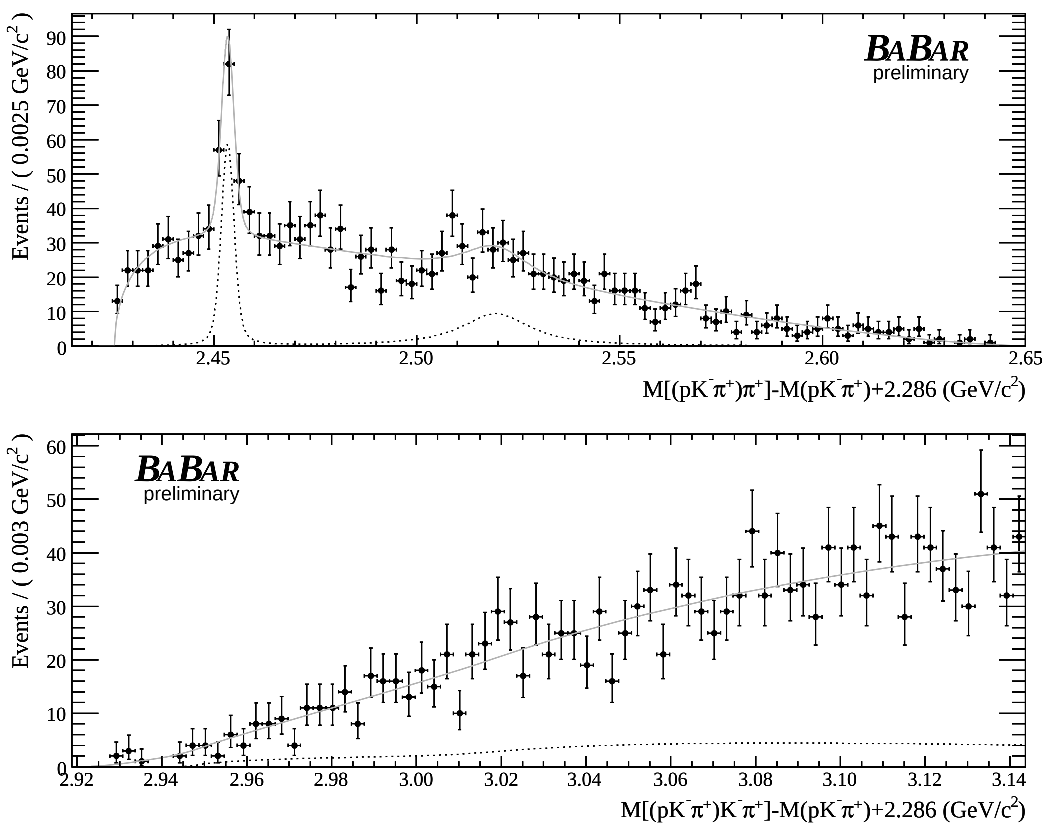

Figure 6: Projections onto the mass variables M_{Σ_c} (upper) and M_{Ξ_c} (lower) of the wrong-sign $\Lambda_c^+ K^+ \pi^-$ data sample (points with error bars) and a fitted PDF (curves) described in the text (Equations 3 and 5). The solid curves represent the total fit PDF. The dotted curves represent the fitted resonant combinatoric background PDF component.

is used to fit the background candidates in the right-sign data sample where the intermediate resonances are now the $\Sigma_c(2455)^{++}$ and the $\Sigma_c(2520)^{++}$.

The signal PDF components used for both the $\Xi_c(2980)^+$ and $\Xi_c(3077)^+$ non-resonant decays are proportional to

$$F_3(M_{\Xi_c}, M_{\Sigma_c}) \times V(M_{\Xi_c}) \,, \tag{7}$$

where $F_3(M_{\Xi_c}, M_{\Sigma_c})$ is a three-body phase-space function and $V(M_{\Xi_c})$ is a Voigtian function in M_{Ξ_c}. The three-body phase space function is

$$F_3(M_{\Xi_c}, M_{\Sigma_c}) = \frac{[(M_{\Xi_c}^2 - (M_{\Sigma_c} + m_K)^2)(M_{\Xi_c}^2 - (M_{\Sigma_c} - m_K)^2)]^{1/2}}{2M_{\Xi_c}} \times F_2(M_{\Sigma_c}) \,, \tag{8}$$

where m_K is the K^+ mass.

The signal PDF components used for both the $\Xi_c(2980)^+$ and $\Xi_c(3077)^+$ decaying through intermediate resonances are proportional to the three-body phase-space function $F_3(M_{\Xi_c}, M_{\Sigma_c})$ times a Voigtian function in M_{Ξ_c} and two Voigtian functions in M_{Σ_c}:

$$F_3(M_{\Xi_c}, M_{\Sigma_c}) \times V(M_{\Xi_c}) \times [(1 - r')V_a(M_{\Sigma_c}) + r'V_b(M_{\Sigma_c})] \,, \tag{9}$$

where the functions $V_a(M_{\Sigma_c})$ and $V_b(M_{\Sigma_c})$ share the same free parameters as those in the background PDF components, and r' is an independent ratio parameter used for the signal PDF component. The $\Xi_c(2980)^+$ cannot decay to $\Sigma_c(2520)^{++}K^-$. In this case, the value of r' is fixed to zero.

Signal-MC samples are used to determine the detector resolution in M_{Ξ_c} and M_{Σ_c}. The measured resolutions for $\Xi_c(2980)^+$ and $\Xi_c(3077)^+$ are $(1.6 \pm 0.1)\,\mathrm{MeV}/c^2$ and $(2.0 \pm 0.1)\,\mathrm{MeV}/c^2$, respectively. The measured resolutions for $\Sigma_c(2455)^{++}$ and $\Sigma_c(2520)^{++}$ are $(1.3 \pm 0.2)\,\mathrm{MeV}/c^2$ and $(1.8 \pm 0.1)\,\mathrm{MeV}/c^2$, respectively.

In the fits to data, the simulated detector resolutions are used as fixed parameters in the Voigtian line shapes. Values of kinematic thresholds are also fixed. All other parameters are free in the fits.

4 SYSTEMATIC STUDIES

Several sources of systematic uncertainty are investigated and quantified. The results are summarized in Tables 1 and 2.

The values of the fixed resolution parameters are changed to determine the effect on the measured mass differences, widths, and yields. The widths of all convolved resolution-Gaussians are increased and decreased by 10% in two additional fits to the data. The largest changes to the mass difference, width, and yield for the $\Xi_c(2980)^+$ signal are $+0.09\,\mathrm{MeV}/c^2$, $-0.5\,\mathrm{MeV}$ and -1%, respectively. The largest changes to the mass difference, width, and yield for the $\Xi_c(3077)^+$ signal are $+0.01\,\mathrm{MeV}/c^2$, $+0.4\,\mathrm{MeV}$ and -2.2%, respectively. The magnitudes of these changes in fitted values are used as symmetric systematic errors. Systematic errors for resonant and non-resonant yields are similarly calculated.

In order to evaluate systematic errors due to the shapes of the threshold PDF components, the exponent (1/2) is allowed to be a free parameter in the fit:

$$\left[-1 + \left(\frac{x}{t}\right)^2\right]^{1/2} \rightarrow \left[-1 + \left(\frac{x}{t}\right)^2\right]^q \,, \tag{10}$$

where q is the new free parameter. There is one new parameter q used for the threshold components in M_{Ξ_c} and a second for the threshold components in M_{Σ_c}. The mass difference, width, and yield for the $\Xi_c(2980)^+$ signal change by $+0.9\,\mathrm{MeV}/c^2$, $-1.1\,\mathrm{MeV}$, and -10%, respectively. The mass difference, width, and yield for the $\Xi_c(3077)^+$ signal change by $+0.0004\,\mathrm{MeV}/c^2$, $+0.17\,\mathrm{MeV}$, and $+0.5\%$, respectively. The magnitudes of these changes in fitted values are used as symmetric systematic errors. Systematic errors for resonant and non-resonant yields are similarly calculated.

The $\Xi_c(2980)^+$ and $\Xi_c(3077)^+$ signals are fit with non-relativistic Breit-Wigner shapes convolved with Gaussian resolution functions in the M_{Ξ_c} variable. We check that there are no substantial errors due to our choice of signal shape. This is done by fitting the $\Xi_c(2980)^+$ and $\Xi_c(3077)^+$ distributions in signal-MC samples with non-relativistic Breit-Wigner and relativistic S-wave Breit-Wigner shapes convolved with Gaussian resolution functions. The largest fractional differences found in the resultant mass difference, width, and yield are 0.019%, 0.018%, and 0.20%, respectively. These fractional changes are used as symmetric systematic errors and are converted into magnitudes in Tables 1 and 2.

The phase-space functions $F_2(M_{\Sigma_c})$ and $F_3(M_{\Xi_c}, M_{\Sigma_c})$ are not convolved with the resolution functions in the M_{Ξ_c} or M_{Σ_c} variables. A systematic error due to this PDF inaccuracy is quantified by shifting the M_{Ξ_c} variable in $F(M_{\Xi_c}, M_{\Sigma_c})$ by $-2.0\,\mathrm{MeV}/c^2$, refitting the data, and taking changes in measured quantities as symmetric systematic errors. Similarly, the M_{Σ_c} variable in $F(M_{\Xi_c}, M_{\Sigma_c})$ and $F(M_{\Sigma_c})$ is shifted by $-1.3\,\mathrm{MeV}/c^2$. Summing these systematic errors in quadrature, the systematic uncertainties for the $\Xi_c(2980)^+$ mass difference, width, and yield are $\pm0.33\,\mathrm{MeV}/c^2$, $\pm0.6\,\mathrm{MeV}$ and $\pm13\%$, respectively. The systematic uncertainties for the $\Xi_c(3077)^+$ mass difference, width, and yield are $\pm0.006\,\mathrm{MeV}/c^2$, $\pm0.21\,\mathrm{MeV}$ and $\pm5.3\%$, respectively. Systematic errors for resonant and non-resonant yields are similarly calculated.

Measurements of particle mass with the *BABAR* detector have systematic errors associated with SVT alignment, detector angular dependencies, energy-loss corrections, the solenoidal magnetic field, and material magnetization. These systematic errors were extensively studied for *BABAR*'s precision measurement of the Λ_c^+ mass [7] and were determined to contribute $\pm0.14\,\mathrm{MeV}/c^2$ total systematic error to the Λ_c^+ mass measurement. The decay mode utilized in the Λ_c^+ mass measurement ($\Lambda K_S^0 K^+$) and the decay mode used in this analysis ($\Lambda_c^+ K^- \pi^+$) have similar Q-values, where the Q-value for a decay $a \rightarrow b + c + \ldots$ is defined as $Q = m_a - m_b - m_c - \ldots$. These similar Q-values, along with our more stringent requirement on candidate momentum, lead us to believe that $\pm0.14\,\mathrm{MeV}/c^2$ is a conservative estimate for the systematic error from detector effects in this analysis.

5 PHYSICS RESULTS

The data is fit to determine $\Xi_c(2980)^+$ and $\Xi_c(3077)^+$ signal widths, mass differences with respect to Λ_c^+, and total yields, as well as yields for resonant and non-resonant decays. Figure 7 shows projections of the data and the fit results. Figure 8 shows the same projections of the data and the fit, but with regions magnified to further illustrate the individual PDF components.

In order to determine the statistical significance of the $\Xi_c(2980)^+$ and $\Xi_c(3077)^+$ signals, fits to the data are performed without each of the signal components for the $\Xi_c(2980)^+$ and the $\Xi_c(3077)^+$. The maximum log likelihood for the fit decreases by 28.9 units when the $\Xi_c(2980)^+$ signal PDF is excluded from the fit. This decrease in maximum log likelihood, with the joint estimation of three parameters (mass, width, and yield), corresponds to a $7.0\,\sigma$ significance for the $\Xi_c(2980)^+$ signal. The maximum log likelihood decreases by 42.5 units when the $\Xi_c(3077)^+$ signal is excluded

Table 1: Systematic errors on $\Xi_c(2980)^+$ and $\Xi_c(3077)^+$ mass differences, widths, and yields due to uncertainties in signal resolution, phase-space kinematic suppression, and the background PDF parameterization. The systematic errors from each source are added in quadrature.

	Mass Difference (MeV/c^2)	Width (MeV)	Yield (%)
$\Xi_c(2980)^+$			
Resolution	± 0.09	± 0.5	± 1
Background Parameters	± 0.88	± 1.1	± 10
Breit-Wigner Shape	± 0.13	< 0.05	< 0.5
Phase-Space	± 0.33	± 0.6	± 13
Detector Effects	± 0.14	—	—
Total	± 0.96	± 1.3	± 16
$\Xi_c(3077)^+$			
Resolution	± 0.01	± 0.44	± 2.2
Background Parameters	< 0.005	± 0.17	± 0.5
Breit-Wigner Shape	± 0.15	< 0.005	± 0.2
Phase-Space	± 0.06	± 0.21	± 5.3
Detector Effects	± 0.14	—	—
Total	± 0.21	± 0.52	± 5.8

Table 2: Systematic errors on $\Xi_c(2980)^+$ and $\Xi_c(3077)^+$ resonant and non-resonant decay yields due to uncertainties in signal resolution, phase-space kinematic suppression, and the background PDF parameterization. The systematic errors from each source are added in quadrature.

	Resolution	Phase-Space	Breit-Wigner	Background	Total
$\Xi_c(2980)^+ \to \Sigma_c(2455)^{++}K^-$	$\pm 2.3\%$	$\pm 1.4\%$	$\pm 0.2\%$	$\pm 2.2\%$	$\pm 3.5\%$
$\Xi_c(2980)^+ \to \Lambda_c^+K^-\pi^+$	$\pm 1.9\%$	$\pm 24.9\%$	$\pm 0.2\%$	$\pm 15.7\%$	$\pm 29.5\%$
$\Xi_c(3077)^+ \to \Sigma_c(2455)^{++}K^-$	$\pm 3.1\%$	$\pm 1.6\%$	$\pm 0.2\%$	$\pm 2.2\%$	$\pm 4.1\%$
$\Xi_c(3077)^+ \to \Sigma_c(2520)^{++}K^-$	$\pm 2.3\%$	$\pm 3.4\%$	$\pm 0.2\%$	$\pm 5.7\%$	$\pm 7.0\%$
$\Xi_c(3077)^+ \to \Lambda_c^+K^-\pi^+$	$\pm 10.6\%$	$\pm 42.0\%$	$\pm 0.2\%$	$\pm 15.7\%$	$\pm 46.1\%$

Table 3: Comparison of masses, widths, yields, and significances for $\Xi_c(2980)^+$ and $\Xi_c(3077)^+$, measured by *BABAR* and Belle in the $\Lambda_c^+ K^- \pi^+$ final state. The quoted Belle significance are calculated assuming the estimation of one parameter; the *BABAR* significances are calculated for the joint estimation of three parameters (mass, width and yield).

	Mass (MeV/c^2)	Width (MeV)	Yield (Events)	Significance
BABAR $\Xi_c(2980)^+$	$2967.1 \pm 1.9 \pm 1.0$	$23.6 \pm 2.8 \pm 1.3$	$284 \pm 45 \pm 46$	$7.0\,\sigma$
Belle $\Xi_c(2980)^+$	$2978.5 \pm 2.1 \pm 2.0$	$43.5 \pm 7.5 \pm 7.0$	405 ± 51	$6.3\,\sigma$
BABAR $\Xi_c(3077)^+$	$3076.4 \pm 0.7 \pm 0.3$	$6.2 \pm 1.6 \pm 0.5$	$204 \pm 35 \pm 12$	$8.6\,\sigma$
Belle $\Xi_c(3077)^+$	$3076.7 \pm 0.9 \pm 0.5$	$6.2 \pm 1.2 \pm 0.8$	326 ± 40	$9.7\,\sigma$

from the fit. This decrease in the maximum log likelihood, again with the joint estimation of three parameters, corresponds to a significance of $8.6\,\sigma$.

The measured mass differences with respect to the Λ_c^+ are

$$M(\Xi_c(2980)^+) - M(\Lambda_c^+) = (680.6 \pm 1.9 \pm 1.0)\,\mathrm{MeV}/c^2\,, \text{and}$$

$$M(\Xi_c(3077)^+) - M(\Lambda_c^+) = (790.0 \pm 0.7 \pm 0.2)\,\mathrm{MeV}/c^2\,.$$

The masses, widths, yields, and significances for the $\Xi_c(2980)^+$ and $\Xi_c(3077)^+$ are listed in Table 3. The $\Xi_c(2980)^+$ and $\Xi_c(3077)^+$ masses are calculated from their mass differences with respect to the Λ_c^+ by adding the Λ_c^+ mass $(2286.46 \pm 0.14)\,\mathrm{MeV}/c^2$ as measured by *BABAR* [7]. The total yields for the $\Xi_c(2980)^+$ and $\Xi_c(3077)^+$ signals are the combined yields from their resonant and non-resonant decays, and take into account the correlations due to the shared mean mass-difference and width parameters. Masses, widths, yields, and significances, as measured by the Belle Collaboration in the $\Lambda_c^+ K^- \pi^+$ final state [1, 2], are also listed for comparison. The quoted Belle significance are calculated assuming the estimation of one parameter.

The yields and significances for the separate resonant and non-resonant decays are listed in Table 4. The significances for the resonant and non-resonant decays of the $\Xi_c(2980)^+$ and $\Xi_c(3077)^+$ are each calculated separately with the same method as for the full signal but with the yield being the only parameter estimated. We find that the signal for the resonant decay $\Xi_c(2980)^+ \to \Sigma_c(2455)^{++} K^-$ has a $4.9\,\sigma$ significance. The signal for the non-resonant decay $\Xi_c(2980)^+ \to \Lambda_c^+ K^- \pi^+$ has a $4.1\,\sigma$ significance. We find that the signal for the resonant decay $\Xi_c(3077)^+ \to \Sigma_c(2455)^{++} K^-$ has a $5.8\,\sigma$ significance, and the signal for $\Xi_c(3077)^+ \to \Sigma_c(2520)^{++} K^-$ has a $4.6\,\sigma$ significance. The signal for the non-resonant decay $\Xi_c(3077)^+ \to \Lambda_c^+ K^- \pi^+$ has a $1.4\,\sigma$ significance.

6 SUMMARY

We analyze $315.7\,\mathrm{fb}^{-1}$ of data collected with the *BABAR* detector and search for $\Xi_c(2980)^+ \to \Lambda_c^+ K^- \pi^+$ and $\Xi_c(3077)^+ \to \Lambda_c^+ K^- \pi^+$. A significant signal is found for the non-resonant decay of $\Xi_c(2980)^+$ to $\Lambda_c^+ K^- \pi^+$ as well as for a resonant decay through $\Sigma_c(2455)^{++} K^-$. Significant signals are found for resonant decays of $\Xi_c(3077)^+$ to $\Lambda_c^+ K^- \pi^+$ through the intermediate states $\Sigma_c(2455)^{++} K^-$ and $\Sigma_c(2520)^{++} K^-$. We find only a small indication that $\Xi_c(3077)^+$ decays non-resonantly to $\Lambda_c^+ K^- \pi^+$. Our measured values of $\Xi_c(3077)^+$ mass and width are consistent with

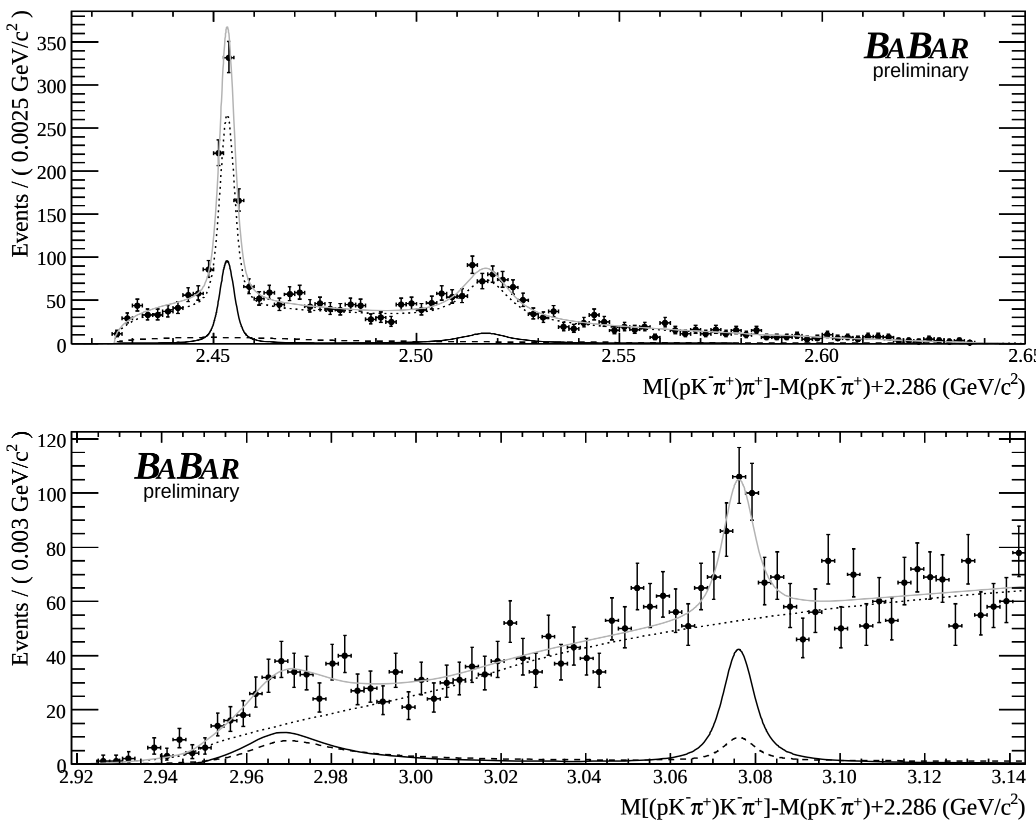

Figure 7: Projections onto the mass variables M_{Σ_c} (upper) and M_{Ξ_c} (lower) for the data (points with error bars) and the fitted two-dimensional PDF (curves). The solid gray curves represent the total fit PDF. The dotted curves represent the sum of the background components with no intermediate resonances and with the $\Sigma_c(2455)^{++}$ and $\Sigma_c(2520)^{++}$ intermediate resonances. The solid dark curves represent the sum of the $\Xi_c(2980)^+ \to \Sigma_c(2455)^{++}K^-$ signal component, the $\Xi_c(3077)^+ \to \Sigma_c(2455)^{++}K^-$ signal component, and the $\Xi_c(3077)^+ \to \Sigma_c(2520)^{++}K^-$ signal component. The dashed curves represent the sum of the $\Xi_c(2980)^+ \to \Lambda_c^+ K^-\pi^+$ and $\Xi_c(3077)^+ \to \Lambda_c^+ K^-\pi^+$ signal components.

Table 4: Yields and significances for the separate resonant and non-resonant decays.

	Yield (Events)	Significance
$\Xi_c(2980)^+ \to \Sigma_c(2455)^{++}K^-$	$132 \pm 31 \pm 5$	$4.9\,\sigma$
$\Xi_c(2980)^+ \to \Lambda_c^+ K^-\pi^+$	$152 \pm 37 \pm 45$	$4.1\,\sigma$
$\Xi_c(3077)^+ \to \Sigma_c(2455)^{++}K^-$	$87 \pm 20 \pm 4$	$5.8\,\sigma$
$\Xi_c(3077)^+ \to \Sigma_c(2520)^{++}K^-$	$82 \pm 23 \pm 6$	$4.6\,\sigma$
$\Xi_c(3077)^+ \to \Lambda_c^+ K^-\pi^+$	$35 \pm 24 \pm 16$	$1.4\,\sigma$

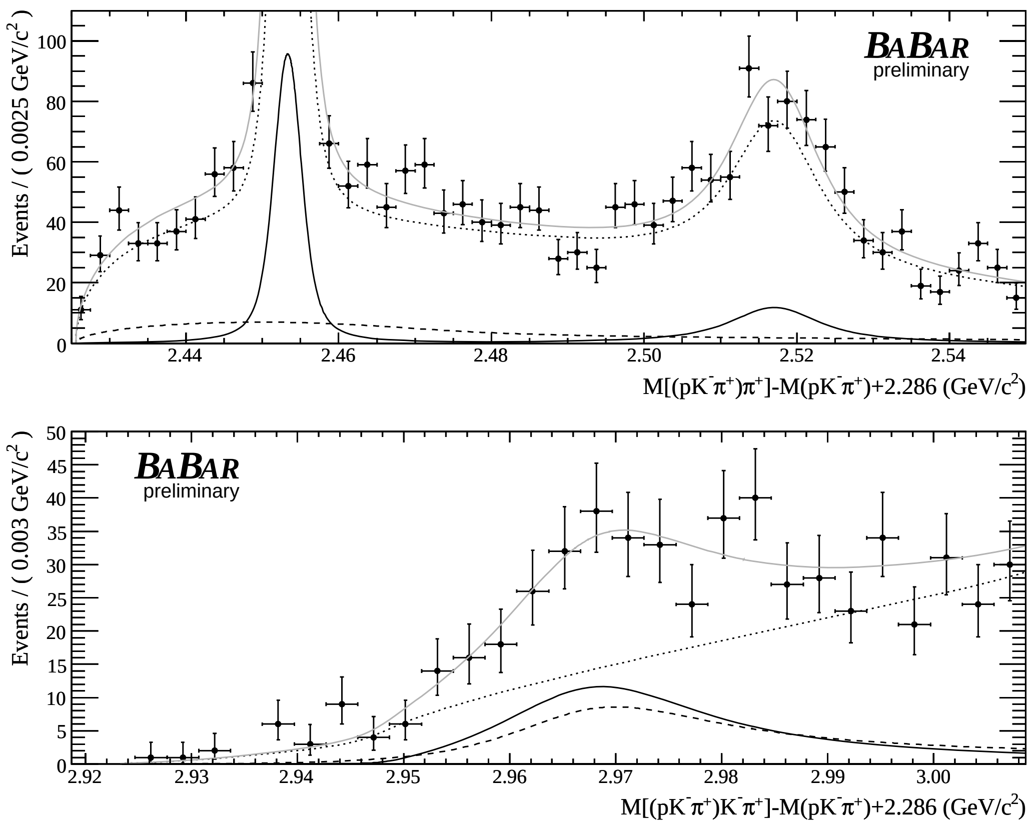

Figure 8: Projections onto the mass variables M_{Σ_c} (upper) and M_{Ξ_c} (lower) for the data (points with error bars) and the fitted PDF (curves), magnified to further illustrate the different PDF components. The curves are the same as in Figure 7. The solid gray curves represent the total fit PDF. The dotted curves represent the sum of the background components with no intermediate resonances and with the $\Sigma_c(2455)^{++}$ and $\Sigma_c(2520)^{++}$ intermediate resonances. The solid dark curves represent the sum of the $\Xi_c(2980)^+ \to \Sigma_c(2455)^{++}K^-$ signal component, the $\Xi_c(3077)^+ \to \Sigma_c(2455)^{++}K^-$ signal component, and the $\Xi_c(3077)^+ \to \Sigma_c(2520)^{++}K^-$ signal component. The dashed curves represent the sum of the $\Xi_c(2980)^+ \to \Lambda_c^+ K^- \pi^+$ and $\Xi_c(3077)^+ \to \Lambda_c^+ K^- \pi^+$ signal components.

results from Belle [1, 2]. However, our measured values of $\Xi_c(2980)^+$ mass and width are significantly lower and narrower, respectively, than those measured by Belle. This may be due to our use of a two-dimensional fit and phase-space considerations.

7 ACKNOWLEDGMENTS

We are grateful for the extraordinary contributions of our PEP-II colleagues in achieving the excellent luminosity and machine conditions that have made this work possible. The success of this project also relies critically on the expertise and dedication of the computing organizations that support *BABAR*. The collaborating institutions wish to thank SLAC for its support and the kind hospitality extended to them. This work is supported by the US Department of Energy and National Science Foundation, the Natural Sciences and Engineering Research Council (Canada), Institute of High Energy Physics (China), the Commissariat à l'Energie Atomique and Institut National de Physique Nucléaire et de Physique des Particules (France), the Bundesministerium für Bildung und Forschung and Deutsche Forschungsgemeinschaft (Germany), the Istituto Nazionale di Fisica Nucleare (Italy), the Foundation for Fundamental Research on Matter (The Netherlands), the Research Council of Norway, the Ministry of Science and Technology of the Russian Federation, Ministerio de Educación y Ciencia (Spain), and the Particle Physics and Astronomy Research Council (United Kingdom). Individuals have received support from the Marie-Curie IEF program (European Union) and the A. P. Sloan Foundation.

References

[1] T. Lesiak [Belle Collaboration], "Charmed baryon spectroscopy with Belle," arXiv:hep-ex/0605047.

[2] R. Chistov *et al.* [Belle Collaboration], "Observation of New States Decaying into $\Lambda_c^+ K^- \pi^+$ and $\Lambda_c^+ K_S^0 \pi^-$," arXiv:hep-ex/0606051.

[3] B. Aubert *et al.* [*BABAR* Collaboration], Nucl. Instrum. Methods **A479**, 1 (2002).

[4] T. Sjostrand, Comput. Phys. Commun. **82**, 74 (1994).

[5] D. J. Lange, Nucl. Instrum. Meth. A **462**, 152 (2001).

[6] S. Agostinelli *et al.* [GEANT4 Collaboration], Nucl. Instrum. Meth. A **506**, 250 (2003).

[7] B. Aubert *et al.* [BABAR Collaboration], "A precision measurement of the Λ_c^+ baryon mass," Phys. Rev. D **72**, 052006 (2005).